

Biofunctional Silicon Nanoparticles by Means of Thiol-Ene Click Chemistry

Loes Ruizendaal,^[a] Sidharam P. Pujari,^[a] Veronique Gevaerts,^[b] Jos M. J. Paulusse,^{*[a]} and Han Zuilhof^{†*[a]}

On the occasion of the 10th anniversary of click chemistry

Abstract: The preparation and characterization of butylene-terminated silicon nanoparticles (SiNPs) and their functionalization using thiol-ene chemistry is described, as well as the coupling of DNA strands. Bromide-terminated SiNPs were prepared by means of the oxidation of magnesium silicide and functionalized with butylene chains through treatment with the corresponding Grignard reagent. The successful coupling was confirmed by NMR and FTIR spectroscopy. TEM measurements revealed a silicon-core diameter of (2.4 ± 0.5) nm. The fluores-

cence emission maximum is at $\lambda_{\text{max}} = 525$ nm when excited at $\lambda_{\text{exc}} = 430$ nm. The conjugation of these alkene-terminated SiNPs by means of thiol-ene chemistry is described for a variety of functional thiols. Efficient coupling was evidenced by NMR and FTIR spectroscopy. Moreover, the characteristic fluorescence properties of the SiNPs remained unaltered, thus demonstrating

the value of this approach towards functional oxide-free SiNPs. Activation of the attached carboxylic acid moieties allowed for conjugation of NH_2 -terminated oligo-ssDNA (ss = single strand) to the SiNPs. Successful coupling was confirmed by a characteristic new UV absorption band at 260 nm, and by the still-present distinctive fluorescence of the SiNPs at 525 nm. Gel electrophoresis confirmed coupling of 2 to 3 DNA strands onto the SiNPs, whereas no uncoupled DNA was observed.

Keywords: bioconjugation • click chemistry • fluorescence spectroscopy • nanoparticles • silicon

Introduction

Bioimaging is essential in gaining a detailed understanding of cellular processes and disease mechanisms. Organic dyes have been successfully employed in the labeling of cells,^[1] but are prone to photobleaching. This severely limits the maximum exposure time,^[2] thus rendering multigeneration staining of cells practically impossible. Quantum dots (QDs) provide an interesting alternative^[3] since they are highly resistant against photobleaching.^[2,4] Furthermore, since the optical properties of QDs are dependent on their size due to

the size-dependent bandgap energy, this allows for tuning of their absorption and fluorescence emission wavelengths.^[5] QDs in biological systems have already found several applications in bioanalysis^[4] and bioimaging.^[2,4,6] These QDs are, however, not tolerant to many common solvents due to the noncovalent manner in which their surface coating is typically attached. Moreover, the inherent toxicity of core atoms like Cd and Pb impedes widespread application in biological environments.^[7] Finally, the total size of typical core-shell QDs, including the typically essential stabilizing polymeric coating, is relatively large (20–50 nm). This affects cell penetration^[8] and the residence time within the organism: only particles smaller than 5 nm in diameter are readily excreted from the body through urinary excretion; larger particles accumulate in the body and are disposed of in other ways.^[8]

Silicon nanoparticles (SiNPs) with sizes smaller than the Bohr exciton radius (≈ 5 nm) have optical properties comparable to conventional QDs.^[9] However, extensive studies have indicated their intrinsic nontoxicity,^[10] depending on the surface charge,^[11] thus demonstrating their potential for imaging in biological systems. The protective organic coating of the SiNPs may be very thin (≈ 0.5 nm), thereby maintain-

[a] L. Ruizendaal, S. P. Pujari, J. M. J. Paulusse, H. Zuilhof
Laboratory of Organic Chemistry
Wageningen University
Dreijenplein 8, 6703 HB Wageningen (The Netherlands)
E-mail: Jos.Paulusse@wur.nl
Han.Zuilhof@wur.nl

[b] V. Gevaerts
Molecular Science and Technology
Eindhoven University of Technology
Den Dolech 2, 5612 AZ Eindhoven (The Netherlands)

Supporting information for this article is available on the WWW under <http://dx.doi.org/10.1002/asia.201100375>.

ing the total diameter at a relatively small size. Several methods to obtain SiNPs have been developed thus far, such as electrochemical dispersion of crystalline silicon,^[12] ultrasonication of silicon wafers,^[13] thermal degradation of silanes in supercritical fluids,^[14] and laser-driven pyrolysis of silanes.^[15] Furthermore, a number of wet-chemical bottom-up approaches have been developed, such as the synthesis in micelles by using organosilanes as silicon source,^[16] and through the reactions with Zintl salts.^[17] These wet-chemical methods typically result in SiNPs that are either hydrogen-terminated or halogen-terminated, and hence highly prone to oxidation. Since oxidation of the SiNPs dramatically affects their optical properties,^[18] passivation of the SiNPs by using terminal alkenes^[16a] or alkyl-lithium reagents^[17a] is essential. The resulting stable Si–C bonds form a stable shell around the Si core and prevent oxidation. However, for application of such SiNPs in selective labeling, functional moieties on the particle are desired.

The development of new and accurate biodiagnostic tools makes the identification of infectious diseases faster and thereby prevents unnecessary illness and loss of lives. Current methods to detect pathogenic bacteria and viruses—such as tuberculosis and influenza—are laborious and time-consuming, since typically an amplification step is involved, which may take several days.^[19] The search for faster tests with even lower detection limits therefore remains important. For DNA and RNA sensing in particular, hybridization of the target sequence with a probe is a commonly employed approach because of its simplicity and effectiveness.^[20] Recently developed nanomaterials for the detection of DNA and RNA—which are based, among others, on magnetic sensing, electronic detection, surface plasmon resonance, or fluorescence spectroscopy^[21]—are highly promising, as they combine fast analysis with high specificity and low detection limits. For these detection systems, the conjugation of biomolecules is crucial. Fluorescence spectroscopy-based detection methods are increasingly employing QDs as the source of fluorescence instead of organic dyes.^[22] This is due to their strongly diminished photobleaching^[2,4] and size-tunable emission wavelength.^[5] The detection of biomolecules in solution with QDs may be achieved in several ways: by making use of Förster resonance energy transfer (FRET), fluorescence quenching, and by changes in the fluorescence anisotropy.^[16a,23] In FRET, the QD acts as a FRET donor onto which a capture molecule is attached; upon binding of the target molecule—that is, DNA or proteins—a FRET acceptor is brought close enough to the donor to display FRET emission.^[24] With this method, sensitive detection of DNA target strands has been achieved.^[25] Analogously, binding of target DNA may bring a fluorescence quencher into the close proximity of a QD,^[26] thereby resulting in loss of fluorescence. Recently, changes in the fluorescence anisotropy of QDs were used to detect binding of a complementary DNA strand to a single-strand DNA-functionalized QD.^[27] The rotation correlation time increased drastically upon hybridization of the complementary DNA strand, since a double-stranded DNA molecule is very

rigid, and thus increases the hydrodynamic radius of the particle accordingly.

The conjugation of biomolecules such as antibodies and proteins with fluorescent labels is of great importance for targeted labeling of certain parts of cells or cell-wall receptors. Jaiswal et al. reported a general method for coating QDs with proteins or antibodies for targeting purposes.^[28] Commercially available QDs were coated with avidin, after which the biotinylated molecule of interest was coupled. Nonetheless, it remains a challenge to prepare QDs that do not remain in clusters but move independently and are efficiently internalized by cells. Due to the relatively large dimensions of QDs (20–50 nm), regular uptake by cells would entail endocytosis. This leads to encapsulated clusters of QDs, which are only barely released from the capsules into the cell.^[29] However, QDs functionalized with targeting peptides have been successfully applied in the specific labeling of cell nuclei,^[6b,30] whereas proteins located in the cytoplasm were specifically labeled by making use of His-tag modified QDs.^[31] Specific labeling of a certain cell type was also accomplished with antibody-coated QDs, which may then bind to membrane receptors. In this way, Nie and co-workers achieved the specific targeting of human prostate tumor cells in mice by coupling prostate-specific membrane antigen monoclonal antibodies onto QDs.^[32] Other examples are the labeling of tumorous cells with peptide-conjugated QDs, as well as the monitoring of diffusion dynamics of single receptors on cell membranes with antibody-coated QDs.^[33] DNA-conjugated QDs are commonly applied in fluorescence in situ hybridization (FISH)^[23] that allows certain parts of chromosomes to be labeled to detect chromosomal defects.^[34]

Direct coupling of functional groups or biomolecules onto SiNPs is not trivial due to the high reactivity of the passivation agent (alkyl lithium reagents or Grignard reagents for bromide-terminated SiNPs), as well as the susceptibility of hydrogen-terminated or halogen-terminated SiNPs towards nucleophilic attack.^[35] Several approaches have been pursued, for example, the use of protective group chemistry^[36] or the use of innocent reactive groups, such as epoxides,^[37] azides,^[10] amines,^[38] or terminal alkenes.^[37] Wang et al. reported on the conjugation of DNA strands onto alkyl-functionalized SiNPs by using a photochemical reaction with an aryldiazirine to activate the alkyl moiety by means of carbene-chemistry.^[39] NHS groups attached in this way were subsequently substituted by amine-terminated single-strand (ss) DNA strands. Gel electrophoresis confirmed attachment of the DNA strands. An alternative promising approach for the functionalization of SiNPs is the use of “click chemistry.” Click reactions are characterized by their mild reaction conditions, the use of benign solvents, high regio- and chemoselectivity, and high yields.^[40] Thiol-ene chemistry, which involves a radical-initiated coupling of a thiol to an alkene, has been known for over a century.^[41] Recently, it has attracted great interest as a click reaction, since it does not require a metal catalyst, proceeds under very mild conditions, and is insensitive to water and oxygen.^[42] The ready availa-

bility of thiol-functional biomolecules is an additional advantage. Several excellent reviews exemplify the many applications of the versatile thiol-ene reaction^[40c, 41b, 42b, 43] Examples of successful application are the modification of surfaces,^[44] polymers,^[45] and the preparation of dendrimeric structures^[46] and soft polymeric stamps;^[47] this reaction was even demonstrated to proceed in sunlight without extra irradiation with UV light.^[45a] The versatility and mild conditions of this reaction prompted us to employ thiol-ene click chemistry in the modification of alkene-terminated SiNPs. In this paper we present the development of alkene-terminated SiNPs, their detailed characterization, and their subsequent functionalization with a variety of functional groups using thiol-ene click chemistry (Scheme 1). Furthermore, the functionalization of carboxylic acid-terminated SiNPs with amine-functional DNA strands is described, and the detailed characterization of the resulting bioconjugates is provided.

Results and Discussion

Alkene-Terminated SiNPs

Bromine-terminated SiNPs were synthesized following an adapted procedure by Kauzlarich and co-workers by means of oxidation of Mg_2Si with bromine.^[17a] Capping these bromine-terminated SiNPs with 3-butenylmagnesium bromide yielded alkene-terminated SiNPs (SiNP-ene, **1**). The resulting SiNPs were purified by size-exclusion chromatography (SEC) with ethyl acetate as eluents to yield per reaction batch SiNPs in 30 mg quantities as an orange waxy material.

The size of the SiNP core was determined by TEM. Figure 1 shows a typical TEM image of **1**; the observed particle size is (2.4 ± 0.5) nm, with a radius-based polydispersity (PDI) of 1.12. (see the Supporting Information) The alkene-terminated SiNPs have a slightly smaller radius than observed earlier for butyl-terminated SiNPs.^[48] This is likely due to the use of SEC instead of silica chromatography as part of the purification procedure. SEC is based on hydrodynamic radius, and may result in a different size distribution than that obtained by a predominantly polarity-based separation.

SiNP-ene (**1**) was characterized by NMR spectroscopy. Figure 2 (top) shows an 1H NMR spectrum in which the $Si-CH_2$ protons result in a signal at $\delta = 0.87$ ppm (Figure 2 a),

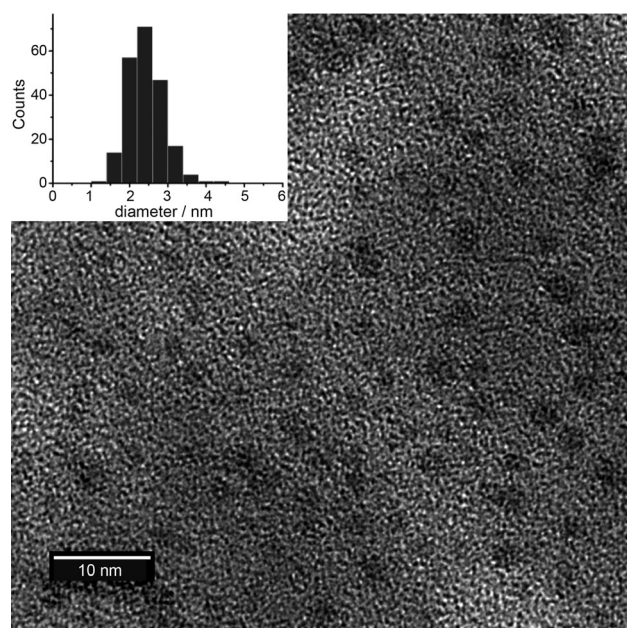
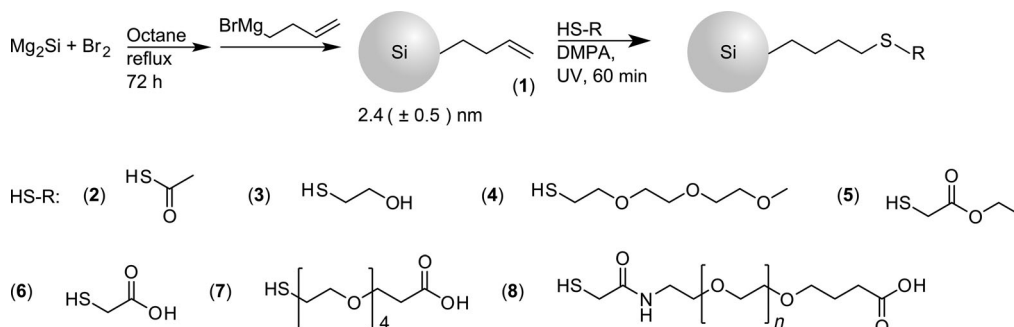


Figure 1. TEM image of alkene-terminated SiNPs (**1**), with corresponding size-distribution histogram (inset).

whereas the double bond protons are observed at $\delta = 4.96$ (Figure 2 c) and $\delta = 5.79$ ppm (Figure 2 d). The observed signal broadening is most likely due to the many different chemical environments of the protons, caused by attachment to different surface sites of the butylene chains. Moreover, due to substantial bromination of the reaction solvent, the attachment of linear and branched octyl chains as well as octyl bromides is also observed ($\delta = 3.5-4.5$ ppm). Diffusion-ordered NMR spectroscopy (DOSY; see the Supporting Information) revealed that the alkene moieties as well as these brominated species are attached to the SiNPs, since they have the same relatively low diffusion coefficient. The low diffusion coefficient (as compared to solvent) indicates that the signal stems from a relatively large moiety, that is, an SiNP. The amount of (brominated) octyl chains was determined by 1H NMR spectroscopy to be butene/octyl = 2.78 (see the Supporting Information). The ^{13}C NMR spectrum (Figure 2, bottom) shows signals that correspond to alkene moieties at $\delta = 112$ ppm (Figure 2 b) and $\delta = 136$ ppm (Figure 2 c), whereas the alkyl chain appears as multiple signals



Scheme 1. Functionalized fluorescent SiNPs obtained by using thiol-ene click chemistry.

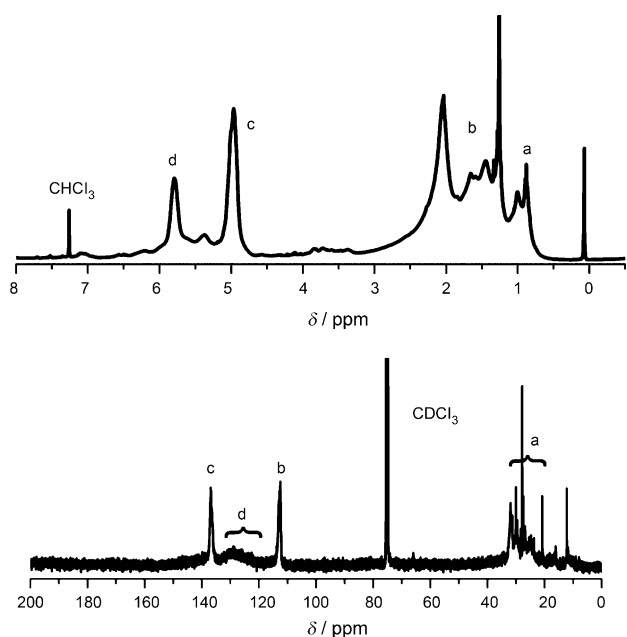


Figure 2. ^1H NMR (top) and ^{13}C NMR (bottom) spectra of SiNP-ene (**1**).

in the $\delta = 21\text{--}31$ ppm region (Figure 2a). The assignment of these signals was confirmed by 2D COSY and 2D heteronuclear single quantum coherence (HSQC) spectra (see the Supporting Information). In the COSY spectrum, protons b and c were confirmed to be positioned on neighboring carbon atoms, furthermore, the $^1\text{H}\text{--}^{13}\text{C}$ HSQC confirms the assignment of carbon atoms a, b, and c in the ^{13}C NMR spectrum, due to coupling with the corresponding signals in the ^1H NMR spectrum. A broad signal at $\delta = 130$ ppm (Figure 2d) in the ^{13}C NMR spectrum indicates the presence of internal alkenes, most likely resulting from elimination reactions that take place on the aforementioned brominated octyl chains due to the Grignard reagent acting as a base.

IR spectroscopy (Figure 3) shows characteristic signals that correspond to the CH_2 groups at 2871 and 2959 cm^{-1} .

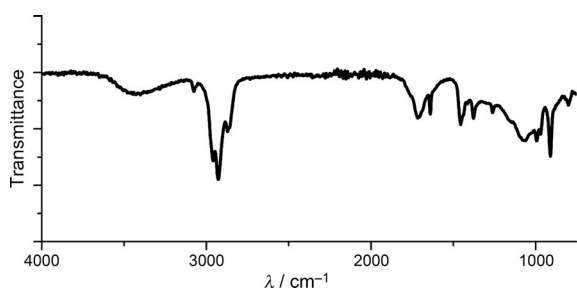


Figure 3. IR spectrum of SiNP-ene (**1**).

Furthermore, the antisymmetric C–H stretch of the alkene moiety is visible at 3077 cm^{-1} . Silicon oxide stretch frequencies are normally observed at approximately $1000\text{--}1100$ cm^{-1} , and characterized by strong signals due to the high polarity of the Si–O bond. The silicon oxide stretch signal in the IR spectrum of the SiNP-ene (**1**) is, however, weak, which indicates that only minor oxidation of the SiNPs took place during synthesis. Since no increases of the Si–O signals were observed for aged samples (several months), the Si core of such butylene-coated SiNPs (**1**) is presumably well protected against further oxidation.

SiNP-ene (**1**) was further characterized by X-ray photoelectron spectroscopy (XPS) to obtain information about the elemental composition. The wide-scan XPS spectrum revealed the presence of silicon (21.1%), carbon (61.7%), bromine (0.4%), and oxygen (16.9%). The oxygen in the sample is most likely largely due to environmental entrapment in the deposited SiNPs within the XPS and not as silicon oxide, since the silicon narrow-scan spectrum displays only a single signal at 101.8 eV, with a full width at half-maximum (FWHM) of 1.3 eV (Figure 4, right), which is near-identical to what is observed under similar instrumental

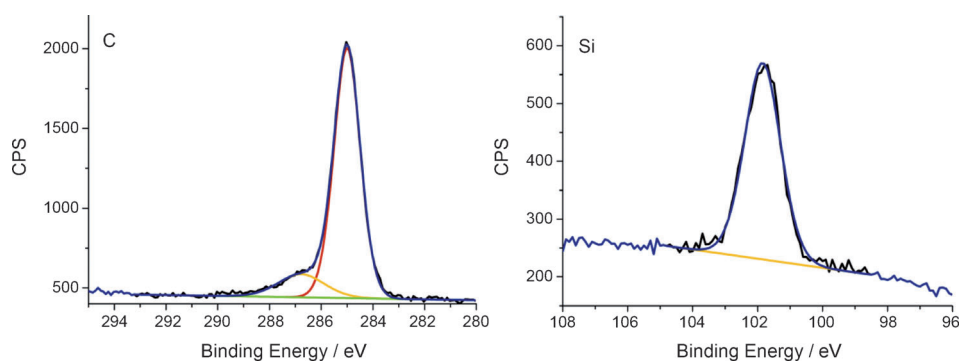


Figure 4. XPS spectra of SiNP-ene (**1**). Left: C_{1s} narrow scan; right: Si_{2p} narrow scan.

conditions for the base peak of Si at 99.4 eV with a FWHM of 0.5 eV in a silicon(111) wafer. The shift in binding energy from 99.4 to 101.8 eV is thus at least partially caused by charging effects, which would indeed be expected for a small object that is well surrounded by an electrically insulating organic shell. Moreover, XPS analysis of samples of intentionally oxidized SiNPs resulted in two signals in the silicon region, the first at 101.8 eV corresponding to silicon, and a second signal at 104.9 eV for silicon oxide (see the Supporting Information). The peak shift is in line with the observation that the binding energy shifts to higher levels with decreasing nanoparticle size relative to bulk silicon.^[49] The narrow scan of the C_{1s} region (Figure 4, left) reveals two types of carbon: carbon-bound carbon at 285.0 eV, and a minor fraction (14%) of carbon atoms bound to electronegative elements such as Br or O (broad shoulder around 287 eV). The precise identity of this peak can, however, not be deduced from XPS analysis alone.

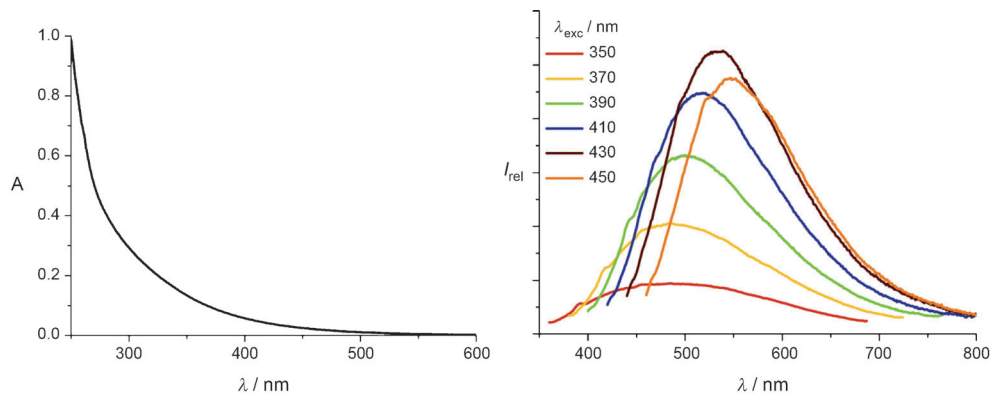


Figure 5. UV/Vis absorption (left) and fluorescence emission map (right) of SiNP-ene (**1**). I_{rel} = relative intensity.

The UV/Vis absorption spectrum of **1** (Figure 5, left) was recorded. However, the spectrum does not display a maximum, it only shows a gradually higher absorption for decreasing wavelengths, as was observed before for this type of SiNPs.^[17a,48] From these samples, the absorption coefficient was determined to be $0.14 \text{ (mg mL}^{-1}\text{)}^{-1}\text{cm}^{-1}$ at 300 nm and $0.035 \text{ (mg mL}^{-1}\text{)}^{-1}\text{cm}^{-1}$ at 350 nm. The extinction coefficient was determined in $\text{(mg mL}^{-1}\text{)}^{-1}\text{cm}^{-1}$, since the exact molecular mass of the SiNP is unknown. Based on a molecular weight of 10000 gmol^{-1} —estimated from TEM measurements in combination with a dense packing of butylene chains—approximate molar extinction coefficients of $3.0 \times 10^2 \text{ M}^{-1}\text{cm}^{-1}$ at 350 nm and $1.4 \times 10^3 \text{ M}^{-1}\text{cm}^{-1}$ at 300 nm were calculated. These values are lower than observed for the 1.5 nm SiNPs prepared by other wet-chemical methods ($9.4 \times 10^3 \text{ M}^{-1}\text{cm}^{-1}$; $1.1 \text{ (mg mL}^{-1}\text{)}^{-1}\text{cm}^{-1}$)^[16a] or for those reported for 1.5 nm QDs of II–VI semiconductors, such as CdSe and CdS ($7 \times 10^4 \text{ M}^{-1}\text{cm}^{-1}$).^[50] However, bulk silicon has an indirect bandgap, which makes optical transitions without the assistance of a phonon inefficient. The optical transition in an SiNP is very efficient in comparison to the transitions in bulk silicon. In the nanometer size regime, the distinction between indirect and direct bandgaps is blurred.^[51]

The fluorescence emission spectrum is strongly dependent on the excitation wavelength. Figure 5 (right) depicts fluorescence emission spectra of **1** at several excitation wavelengths that range from 350 to 450 nm. The spectra are corrected for the UV/Vis absorption at each excitation wavelength. The relatively highest fluorescence emission is observed at 525 nm at an excitation wavelength of 430 nm. This is distinctly redshifted as compared to butyl-terminated SiNPs described previously,^[17a] which showed an emission maximum at 390 nm (obtained for irradiation at 340 nm). For SiNPs with a gradual increase in UV/Vis absorption at shorter wavelengths, correction for UV/Vis absorption results in a redshifted fluorescence emission maximum.

The fluorescence quantum yield (QY) was determined using a comparative method^[23,52] at λ_{exc} = 350, 366, and 496 nm. These dyes have a fluorescence emission that broadly overlaps the fluorescence emission of the SiNPs.

The QYs are $(1.5 \pm 0.2) \%$ and $(1.8 \pm 0.3) \%$ for λ_{exc} = 350 nm and 366 nm, respectively. The QY increases further with increasing excitation wavelength; the highest QY is observed at an excitation wavelength of 496 nm, and is $(7.1 \pm 1.2) \%$. This is about 2% higher than observed for highly similar butyl-terminated SiNPs,^[48] but still considerably smaller than the highest QY reported for SiNPs (60%).^[53] It has been suggested that a high oxidation grade of the SiNPs results in lower quantum yields,^[54] however, such high degrees of oxidation are absent in this case as follows from IR and XPS data. The larger size (2.5 nm in this case) is therefore a more likely cause.

Time-resolved fluorescence spectroscopy was performed, and the amplitude-weighted fluorescence lifetime (see the Supporting Information) was determined to be 3.40 ns, which is similar to the lifetimes observed for butyl-terminated SiNPs.^[48] These results indicate that the optical properties of the SiNPs are not significantly influenced by the change in coating from butyl to butylene.

Thiol-Ene Functionalization of Alkene-Terminated SiNPs

With the alkene moieties present on the surface of the SiNPs, functionalization by means of thiol-ene chemistry is possible. Functional groups may be attached, which make the SiNPs suitable for applications that require specific labels. The SiNPs were mixed with an excess amount of the respective thiol and 0.2 equiv (with respect to the thiol) of 2,2-dimethoxy-2-phenylacetophenone (DMPA) as photoinitiator or 4,4'-azobis(4-cyanovaleric acid) (ACVA) as thermal initiator. The mixture was exposed to UV light (DMPA, 365 nm) or heated to 80 °C (ACVA) while stirring under ambient atmosphere. After 1 h, ¹H NMR spectroscopy revealed complete conversion of the alkene moieties, and the functionalized SiNPs were purified by means of SEC. A number of thiols with different functionalities was selected: thiolacetic acid (SiNP-TAA, **2**) and 2-mercaptoethanol (SiNP-OH, **3**)—which provide for a functional group that may be used in further conjugation reactions—as well as thiolated triethylene glycol monomethyl ether (SiNP-EO₃, **4**), to render the SiNPs water-soluble and biocompatible. Furthermore,

carboxylic acid terminated thiols with three different spacer lengths (no spacer (**6**), an EO₄ spacer (**7**), and a PEG3000 spacer (**8**)) were coupled to the SiNPs to obtain functional groups available for bioconjugation on the surface of the SiNPs (Scheme 1).

The functionalized SiNPs **2**, **3**, **4**, **6**, **7**, were purified by means of SEC, whereas pegylated SiNPs (**8**) were purified with a Amicon Ultra 3K nominal weight cutoff (NWCO) centrifugal units. To obtain SiNP-TGA (**6**), direct coupling of thioglycolic acid is possible and results in full conversion by means of the thiol-ene reaction. However, it appeared that the SiNP-TGA (**6**) obtained in this manner could not be purified. Therefore, the ethyl ester-protected SiNP-TGAEE (**5**) was hydrolyzed with potassium *tert*-butoxide (KO*t*Bu) to obtain thioglycolic acid-modified SiNPs (SiNP-TGA, **6**). The sample was neutralized and purified by evaporation of the solvents.

In the ¹H NMR spectrum of purified SiNP-TAA (**2**) (Figure 6), no terminal alkenes are observed. Furthermore,

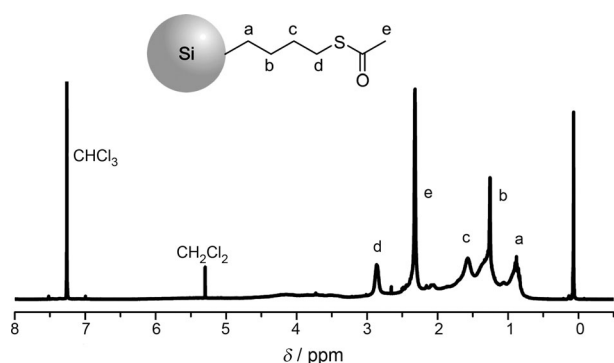


Figure 6. ¹H NMR spectrum of SiNP-TAA (**2**).

a new signal at $\delta = 2.86$ ppm (Figure 6d) corresponds to the newly formed thioester; signals that correspond to the CH₂ next to the thioester appear at $\delta = 1.57$ ppm (Figure 6c), whereas the signal of the methyl group next to the carbonyl appears at $\delta = 2.32$ ppm (Figure 6e).

The ¹H NMR spectrum of SiNP-TGAEE (**5**) (Figure 7) displays characteristic signals of the newly formed thioether

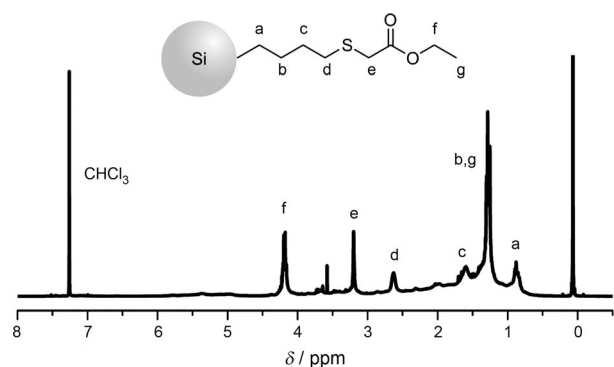


Figure 7. ¹H NMR spectra of SiNP-TGAEE (**5**).

at $\delta = 2.62$ ppm (Figure 7d) (CH₂-CH₂-S) and $\delta = 3.19$ ppm (Figure 7e) (S-CH₂-COOEt). The signals of the ethyl ester moiety were observed at $\delta = 4.17$ ppm (Figure 7f) and $\delta = 1.26$ ppm (Figure 7g), which correspond to the CH₂ and CH₃, respectively. After hydrolysis with KO*t*Bu, these signals are no longer present. The NMR spectra of the thiol-ene-modified SiNPs were assigned with 2D COSY NMR spectroscopy, and in all cases confirm quantitative coupling of the indicated thiols to the SiNPs, since no terminal alkenes are observed after modification, whereas the intensities of the new signals fit accordingly. ¹H NMR spectra of other modified SiNPs can be found in the Supporting Information.

Infrared spectroscopy was performed on the SiNPs to confirm the presence of the characteristic groups and to determine whether the functionalized SiNPs retained their low oxidation grade (Figure 8). The C=CH₂ antisymmetric

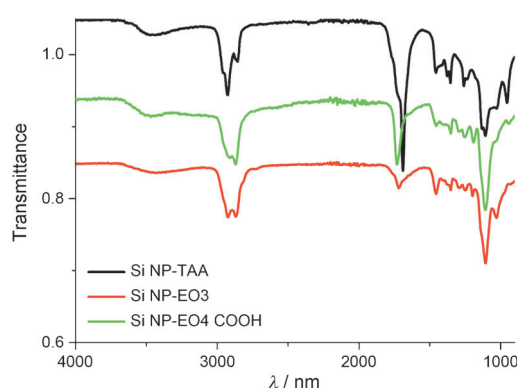


Figure 8. FTIR spectra of SiNPs **2**, **4**, and **7**. FTIR spectra of SiNP **3**, **5**, **6**, and **8** can be found in the Supporting Information.

stretch signal, which appeared at 3077 cm⁻¹ in the case of SiNP-ene, was absent in the spectra of the functionalized SiNPs. All functionalized SiNPs display the typical symmetric and antisymmetric stretch vibrations for CH₂ bonds. Signals for the attached functional groups are readily observed. SiNP-TAA (**2**), for example, displays a distinct carbonyl stretch signal at 1690 cm⁻¹, which confirms the presence of a thioester. SiNP-OH (**3**) displays a broad OH stretch vibration at 3354 cm⁻¹, whereas SiNP-EO₃ (**4**) displays characteristic ether bonds at 1108 cm⁻¹. The spectra of SiNP-TGAEE (**5**), SiNP-TGA (**6**), and SiNP-EO₄-COOH (**7**) display distinct carbonyl stretch signals at 1732 cm⁻¹. The signal is, however, hardly observed in the case of SiNP-PEG3000-COOH (**8**), most likely due to the large amount of ether groups (approximately 170 per chain, at 1103 cm⁻¹) relative to other characteristic groups present in the sample. The presence of ether groups also results in broadening of the signals for the CH₂ symmetric and antisymmetric stretch (they appear as a single peak at 2880 cm⁻¹). In the IR spectrum of SiNP-EO₄-COOH (**7**) the characteristic ether bonds are observed at 1108 cm⁻¹. Importantly, the signal that corresponds to Si-O (1000–1100 cm⁻¹) continues to be weak in all spectra, despite the high polarity of the Si-O bond. This

indicates that even upon performing the radical-based thiol-ene coupling the low degree of oxidation of the Si core is maintained, thus providing further proof of the passivating nature of the organic coating.

The SiNPs were further characterized by using XPS to obtain an elemental composition of the SiNPs, as well as characterizing the different functional groups. A thin film of SiNP-TAA (**2**) was cast onto a gold surface and analyzed.

The XPS narrow scan spectrum of the C_{1s} region of **2** was fit with four components, of which the main peak at 285.0 eV is assigned to carbon-bound carbon atoms (Figure 9, left). The

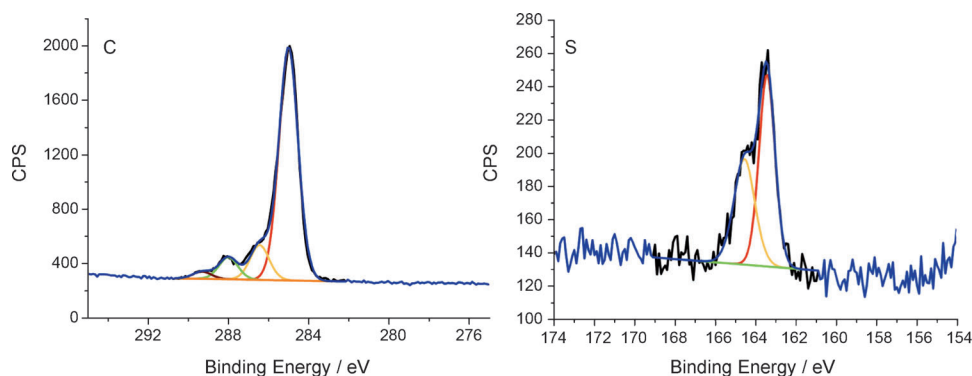


Figure 9. XPS spectra of SiNP-TAA (**2**). Left: C_{1s} narrow scan; right: S_{2p} narrow scan.

intensity of this signal is relatively high (78% of the total carbon content), due to the earlier mentioned side reactions that occur, thereby leading to substantial attachment of alkyl chains (see the Supporting Information). The signals for the C=O (288.0 eV) and C-S (286.4 eV) carbon atoms integrate to a 1:1 ratio. The signal at 289.3 eV (2% of the C_{1s} total area) may arise from slight oxidation of the C=C bond. The XPS narrow scan of the Si_{2p} region (Figure 9, center) reveals only a single signal at 101.8 eV, similar to that observed for SiNP-ene (**1**). The sulfur region shows a clear signal of a single type of sulfur, which was fit with a single spin-orbital doublet (Figure 9, right), in agreement with the thioether that results from the attachment step. XPS spectra of other modified SiNPs can be found in the Supporting Information.

To determine whether the SiNPs retain their optical properties after thiol-ene functionalization, the UV/Vis absorption spectra were recorded (Figure 10, left). As evidenced by the spectra, with normalized absorption at 320 nm, the absorption is not significantly affected by the modification of the SiNPs. This confirms that the Si core remains unaltered under thiol-ene coupling conditions. In addition, fluo-

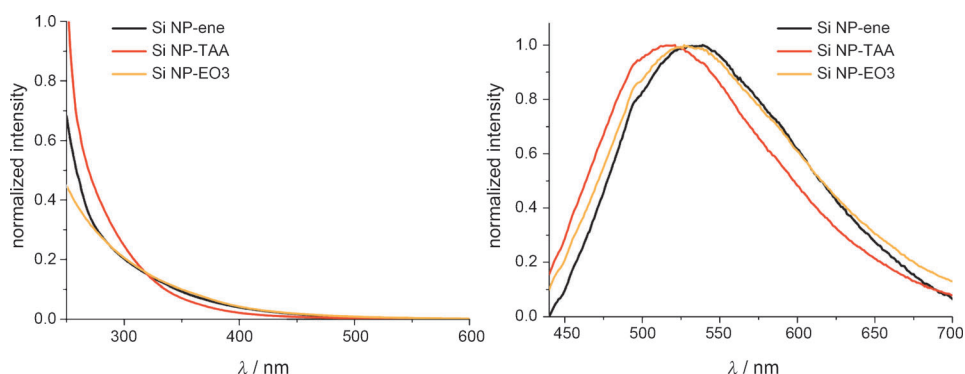


Figure 10. UV/Vis absorption spectra (left) and fluorescence emission (right) of SiNPs **1**, **2**, and **4**. Spectra of SiNPs **3**, **5**, **6**, **7**, and **8** can be found in the Supporting Information.

rescence emission spectra were recorded. In Figure 10 (right), the UV/Vis absorption-normalized fluorescence emission spectra of SiNPs excited at 430 nm are shown, at

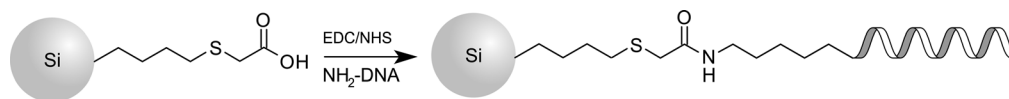
which excitation wavelengths is obtained. The fluorescence emission maxima do not shift significantly for the modified SiNPs and remain at 525 nm. The signal intensity, however, does change to some degree. A slight shift in maximum is observed when comparing SiNP-PEG3000-COOH (**8**) and the other functionalized SiNPs. This is likely as a result of the size-based purification process of **8**, which may alter the size distribution of the SiNPs. Since the fluorescence

emission of SiNPs is size-dependent, changes in the size distribution consequently result in changes in the fluorescence emission maxima.^[15b] This shift is not expected to result from the thiol-ene conjugation, since fluorescence originates from the Si core, with only a small electronic coupling to the covering organic layer, which is unlikely to extend to the distance at which the conjugation reaction takes place.^[55]

Besides steady-state fluorescence spectroscopy, time-resolved fluorescence emission was studied as well. The Supporting Information summarizes the amplitude-weighted averages of the fluorescence lifetimes of the functional SiNPs excited at 372 nm. The results are all in the same time range (≈ 4 ns), thereby further confirming that thiol-ene modification does not significantly affect the SiNPs.

DNA Conjugation

To obtain biofunctional SiNPs with possible applications in biosensors, single-strand deoxyribonucleic acid (ssDNA) with a length of 100 bases with a 3'-amino modification was coupled to the SiNPs by using 1-ethyl-3-(3-dimethylamino-propyl)carbodiimide and *N*-hydroxysuccinimide (EDC/

Scheme 2. ssDNA attachment onto SiNPs by means of EDC/NHS chemistry (example shown: SiNP-TGA (**6**)).

NHS) chemistry (Scheme 2). Samples were purified with 50 k NWCO Amicon centrifugal filter units. Control experiments revealed that both uncoupled ssDNA and uncoupled SiNPs readily pass through 50 k NWCO filters, as evidenced by UV/Vis absorption spectroscopy.

After coupling of the ssDNA and subsequent purification to obtain ssDNA-functionalized SiNPs, the amount of DNA in the NP sample was determined by UV/Vis absorption measurements to determine its concentration. The complementary 3'-Atto 488 dye-modified ssDNA strand was added (1.5 equiv) and incubated at 80 °C for 1 min, after which the sample was allowed to cool to room temperature followed by cooling on ice. Excess amounts of complementary ssDNA were removed by filtration over a 50 k NWCO Amicon centrifugal filter unit. This resulted in double-strand (ds) DNA-modified SiNPs SiNP-TGA-dsDNA (**9**), SiNP-EO₄-dsDNA (**10**), and SiNP-PEG-dsDNA (**11**) (Figure 11).

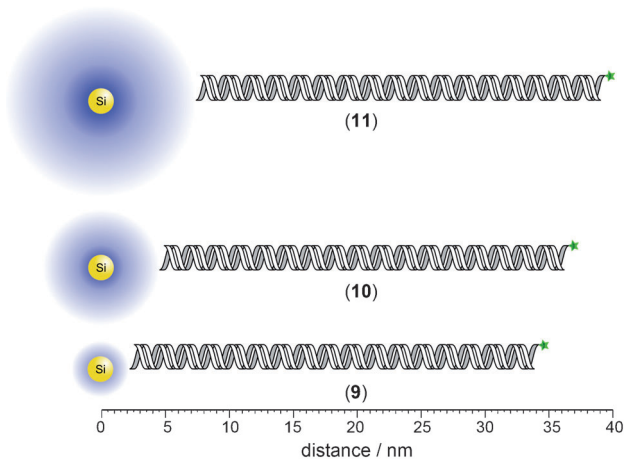
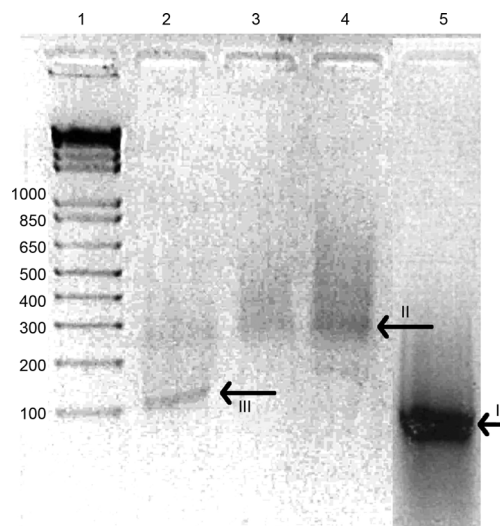


Figure 11. Schematic representation of SiNPs conjugated to a dsDNA strand; complementary strand contains a 3'-Atto 488 dye. (Dimensions scaled, spacers in blue.)

To confirm coupling of the DNA strands to the SiNPs, gel electrophoresis on an agarose gel was performed. Figure 12 shows the agarose gel after a run time of 1 h. Lane 1 contains the reference ladder; the numbers correspond to the number of base pairs (bp) in the respective band. Lane 2 contains SiNP-TGA-dsDNA (**9**); lane 3 SiNP-EO₄-dsDNA (**10**); and lane 4 contains SiNP-PEG-dsDNA (**11**). Lane 5 is a reference lane that contains uncoupled dsDNA (100 bp) with the same sequence as the strands coupled to the NPs. The band in lane 5 runs slightly lower than the 100 bp ladder reference (Figure 12, arrow I). No DNA of this length is observed in lanes 3 and 4, thus indicating successful

Figure 12. Agarose gel with dsDNA-modified SiNPs. Lane 1: 1 kb+ ladder; lane 2: SiNP (**9**); lane 3: SiNP (**10**); lane 4: SiNP (**11**); lane 5: uncoupled 100 bp dsDNA.

purification of the conjugated SiNPs. The heights of the bands in lanes 3 and 4 correspond to approximately 300 bp (Figure 12, arrow II). The SiNPs to which the DNA are coupled are of a specific size, which may influence the height of the band slightly. As such, the bands are proposed to indicate the presence of two to three DNA strands per NP for SiNP-EO₄-dsDNA (**10**) and SiNP-PEG-dsDNA (**11**). A slightly less distinct band at the same height is observed in lane 2, which indicates that in the SiNP-TGA-dsDNA (**9**) sample, up to three strands are also attached to the SiNP. The clearer band in lane 2 just above the 100 bp level (Figure 12, arrow III) most likely corresponds to SiNP-TGA-dsDNA (**9**) with only a single dsDNA strand attached. Tailing of the bands may be due to the range of NP sizes present in the samples (due to a different number of polymeric chains attached), or different numbers or orientations of DNA strands on the SiNPs, thereby resulting in differently sized DNA-functional particles.

UV/Vis absorption and fluorescence emission data of the DNA-modified samples with different spacer lengths unfortunately do not display characteristics that allow for differentiation. The UV/Vis absorption spectrum of the pegylated SiNPs conjugated to ssDNA is shown in Figure 13 (left). However, the main absorption observed originates from the DNA. This points to attachment of the DNA strands to the SiNP, since otherwise these would have been removed in the purification process. The absorption of the SiNP core is still observed when ssDNA is conjugated to the particle, albeit only as a minor contribution, since the ex-

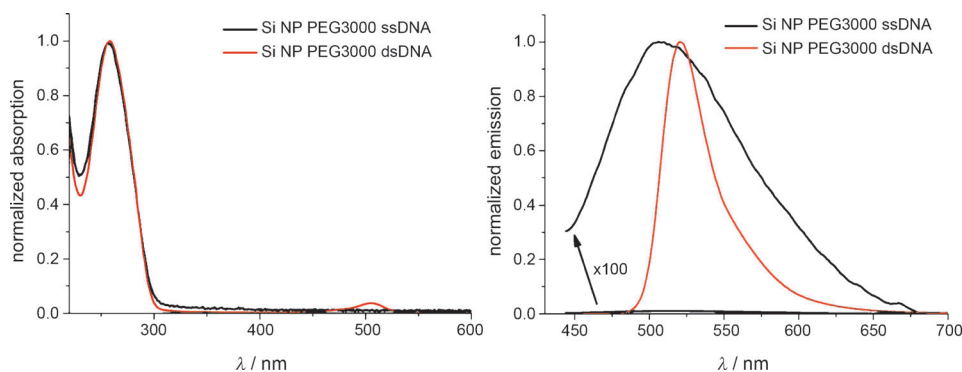


Figure 13. Left: normalized UV/Vis absorption of SiNP-PEG-ssDNA and dsDNA (**11**). Right: normalized fluorescence emission of SiNP-PEG-ssDNA ($\lambda_{\text{exc}} = 430$ nm) and SiNP-PEG-dsDNA (**11**) ($\lambda_{\text{exc}} = 501$ nm).

tion coefficient of ssDNA ($9.8 \times 10^5 \text{ M}^{-1} \text{ cm}^{-1}$, for this particular sequence) is approximately 1000-fold higher than that of the SiNPs at 350 nm ($\approx 3 \times 10^2 \text{ M}^{-1} \text{ cm}^{-1}$). Furthermore, the fluorescence emission of the SiNPs with ssDNA is still observed, although again as a relatively small signal (Figure 13, right). Fluorescence emission contributions from the SiNP core as well as the UV absorption of the ssDNA moiety, indicate that both the SiNPs and ssDNA are present in the sample.

The UV absorption spectrum of the SiNPs that contain dsDNA (**9**, **10**, **11**) is shown in Figure 13 (left). The spectrum is dominated by the absorption of dsDNA and additionally the Atto 488 dye. This is similar to the ssDNA SiNP samples due to the high extinction coefficient for dsDNA ($1.6 \times 10^6 \text{ M}^{-1} \text{ cm}^{-1}$, for this particular sequence). The fluorescence emission of the Atto 488 dye fully dominates the fluorescence spectra of the samples that contain dsDNA-conjugated SiNPs (Figure 13, right).

The fluorescence contribution of the Atto dye indicates that the complementary strand is indeed hybridized to the DNA strand present on the SiNP. The dominance of the Atto 488 dye in the fluorescence spectra with dsDNA is due to the rather low quantum yield (QY) of the SiNPs (7%), whereas the QY of the Atto 488 dye is 80%. Figure 13 (right) shows the UV/Vis absorption and fluorescence emission of SiNP-dsDNA. The spectra are dominated by the absorption and emission of the coupled dsDNA strands and the Atto 488 dye. This indicates that the fluorescent dye is indeed coupled to the SiNPs through the complementary DNA strand, since all uncoupled DNA strands are removed by purification as observed by gel electrophoresis.

Conclusion

The synthesis of silicon nanoparticles (SiNPs) by means of the oxidation of Mg_2Si and subsequent capping with 3-butenylbromide resulted in alkene-functionalized SiNPs with a silicon core size of $2.4 (\pm 0.5)$ nm. Thiol-ene chemistry performed on these SiNPs proved to be a facile, efficient, and versatile approach to obtain a variety of functional SiNPs,

such as those terminated with thioacetic acid, mercaptoethanol, ethylene glycol, and carboxylic acid. The functionalization retains the low degree of oxidation obtained for such NPs and does not change the optical properties of the functionalized SiNPs, which is in line with the Si core being the origin of the optical properties of the SiNPs. Coupling of amine-terminated DNA to the carboxylic acid-terminated SiNPs was confirmed by UV/Vis absorption and fluores-

cence spectroscopy, which indicated both the presence of DNA and SiNPs in the purified samples. Addition of a fluorescently labeled complementary DNA strand yielded SiNPs with two to three covalently coupled dsDNA strands, as confirmed by UV/Vis absorption and fluorescence spectroscopy and by gel electrophoresis. These results demonstrate the successful bioconjugation of DNA onto SiNPs. The employed coupling technique is very mild, and the presented concept is therefore readily extended to proteins or other biomolecules, thus bringing the application of biofunctional SiNPs in sensing devices within reach.

Experimental Section

Experimental details can be found in the Supporting Information. In brief, the SiNPs were synthesized under an argon atmosphere by the oxidation of Mg_2Si by Br_2 while heating to reflux in octane for 72 h. Subsequently, freshly synthesized 4-bromo-1-butene in THF was added to obtain alkene-terminated SiNPs. The SiNPs were purified by extraction and size-exclusion chromatography. For the thiol-ene reaction, in general, an excess amount of the thiol and the radical initiator (0.2 equiv) with respect to the thiol were added to a solution of SiNP-ene (**1**; 10 mg) (approx. 0.1 mmol alkene groups as determined by ^1H NMR spectroscopy with an internal standard) in chlorobenzene or DMF. The reaction was stirred at room temperature while being exposed to UV light (365 nm) (DMPA) or stirred at 80°C to activate the thermal initiator (ACVA), under ambient atmosphere. The resulting SiNPs were purified by size-exclusion chromatography. Coupling of DNA strands was performed under sterile conditions by adding an excess amount of EDC/HCl to SiNPs terminated with carboxylic acid, followed by the addition of NH_2 -terminated ssDNA. Samples were purified with Amicon centrifugal filters.

Acknowledgements

The authors thank Anke Trilling (Wageningen University) for experimental assistance and stimulating discussions. This work was funded by the Dutch Ministry of Economic Affairs within the MicroNed innovation program (WP 2-C-II).

[1] J. B. Pawley, *Handbook of Biological Confocal Microscopy*, Springer, 2006.

- [2] X. Wu, H. Liu, J. Liu, K. N. Haley, J. A. Treadway, J. P. Larson, N. Ge, F. Peale, M. P. Bruchez, *Nat. Biotechnol.* **2003**, *21*, 41–46.
- [3] V. Biju, T. Itoh, M. Ishikawa, *Chem. Soc. Rev.* **2010**, *39*, 3031–3056.
- [4] M. Bruchez, Jr., M. Moronne, P. Gin, S. Weiss, A. P. Alivisatos, *Science* **1998**, *281*, 2013–2016.
- [5] a) A. P. Alivisatos, *Science* **1996**, *271*, 933–937; b) L. Brus, *J. Phys. Chem.* **1986**, *90*, 2555–2560.
- [6] a) K.-T. Yong, H. Ding, I. Roy, W.-C. Law, E. J. Bergey, A. Maitra, P. N. Prasad, *ACS Nano* **2009**, *3*, 502–510; b) A. M. Derfus, W. C. W. Chan, S. N. Bhatia, *Adv. Mater.* **2004**, *16*, 961–966; c) D. S. Lidke, P. Nagy, R. Heintzmann, D. J. Arndt-Jovin, J. N. Post, H. E. Grecco, E. A. Jares-Erijman, T. M. Jovin, *Nat. Biotechnol.* **2004**, *22*, 198–203; d) P. Mitchell, *Nat. Biotechnol.* **2001**, *19*, 1013–1017; e) W. C. W. Chan, S. M. Nie, *Science* **1998**, *281*, 2016–2018.
- [7] a) A. M. Derfus, W. C. W. Chan, S. N. Bhatia, *Nano Lett.* **2004**, *4*, 11–18; b) N. Lewinski, V. Colvin, R. Drezek, *Small* **2008**, *4*, 26–49.
- [8] H. Soo Choi, W. Liu, P. Misra, E. Tanaka, J. P. Zimmer, B. Itty Ipe, M. G. Bawendi, J. V. Frangioni, *Nat. Biotechnol.* **2007**, *25*, 1165–1170.
- [9] a) N. Shirahata, *Phys. Chem. Chem. Phys.* **2011**, in press; b) Z. Kang, Y. Liu, S.-T. Lee, *Nanoscale* **2011**, *3*, 777–791.
- [10] L. Ruizendaal, S. Bhattacharjee, K. Pournazari, M. Rosso-Vasic, L. H. J. De Haan, G. M. Alink, A. T. M. Marcelis, H. Zuilhof, *Nanotoxicology* **2009**, *3*, 339–347.
- [11] S. Bhattacharjee, L. H. J. de Haan, N. M. Evers, X. Jiang, A. T. M. Marcelis, H. Zuilhof, I. M. C. M. Rietjens, G. M. Alink, *Part. Fibre Toxicol.* **2010**, *7*, 25.
- [12] E. V. Rogozhina, D. A. Eckhoff, E. Gratton, P. V. Braun, *J. Mater. Chem.* **2006**, *16*, 1421–1430.
- [13] a) Z. Yamani, S. Ashhab, A. Nayfeh, W. H. Thompson, M. Nayfeh, *J. Appl. Phys.* **1998**, *83*, 3929–3931; b) J. L. Heinrich, C. L. Curtis, G. M. Credo, K. L. Kavanagh, M. J. Sailor, *Science* **1992**, *255*, 66–68.
- [14] a) J. D. Holmes, K. J. Ziegler, R. C. Doty, L. E. Pell, K. P. Johnston, B. A. Korgel, *J. Am. Chem. Soc.* **2001**, *123*, 3743–3748; b) D. S. English, L. E. Pell, Z. Yu, P. F. Barbara, B. A. Korgel, *Nano Lett.* **2002**, *2*, 681–685.
- [15] a) X. Li, Y. He, S. S. Talukdar, M. T. Swihart, *Langmuir* **2003**, *19*, 8490–8496; b) F. Huisken, G. Ledoux, O. Guillois, C. Reynaud, *Adv. Mater.* **2002**, *14*, 1861–1865.
- [16] a) M. Rosso-Vasic, E. Spruijt, B. van Lagen, L. De Cola, H. Zuilhof, *Small* **2008**, *4*, 1835–1841; b) J. H. Warner, A. Hoshino, K. Yamamoto, R. D. Tilley, *Angew. Chem.* **2005**, *117*, 4626–4630; *Angew. Chem. Int. Ed.* **2005**, *44*, 4550–4554; c) J. P. Wilcoxon, G. A. Samara, *Appl. Phys. Lett.* **1999**, *74*, 3164–3166; d) J. P. Wilcoxon, G. A. Samara, P. N. Provencio, *Phys. Rev. B* **1999**, *60*, 2704–2714; e) R. D. Tilley, J. H. Warner, K. Yamamoto, I. Matsui, H. Fujimori, *Chem. Commun.* **2005**, 1833–1835; f) J. Zou, P. Sanelle, K. A. Pettigrew, S. M. Kauzlarich, *J. Cluster Sci.* **2006**, *17*, 565–578.
- [17] a) K. A. Pettigrew, Q. Liu, P. P. Power, S. M. Kauzlarich, *Chem. Mater.* **2003**, *15*, 4005–4011; b) Q. Liu, S. M. Kauzlarich, *Mater. Sci. Eng. B* **2002**, *96*, 72–75; c) D. Neiner, H. W. Chiu, S. M. Kauzlarich, *J. Am. Chem. Soc.* **2006**, *128*, 11016–11017; d) D. Mayeri, B. L. Phillips, M. P. Augustine, S. M. Kauzlarich, *Chem. Mater.* **2001**, *13*, 765–770; e) X. M. Zhang, D. Neiner, S. Z. Wang, A. Y. Louie, S. M. Kauzlarich, *Nanotechnology* **2007**, *18*, 095601.
- [18] G. Ledoux, O. Guillois, D. Porterat, C. Reynaud, F. Huisken, B. Kohn, V. Paillard, *Phys. Rev. B* **2000**, *62*, 15942.
- [19] a) R. S. Wallis, M. Pai, D. Menzies, T. M. Doherty, G. Walzl, M. D. Perkins, A. Zumla, *Lancet* **2010**, *375*, 1920–1937; b) P. Tallury, A. Malhotra, L. M. Byrne, S. Santra, *Adv. Drug Delivery Rev.* **2010**, *62*, 424–437; c) H. Takahashi, Y. Otsuka, B. Patterson, *J. Infect. Chemother.* **2010**, *16*, 155–161.
- [20] A. Merkoçi, *Biosens. Bioelectron.* **2010**, *26*, 1164–1177.
- [21] C. Kumar, *Nanomaterials for Biosensors*, Wiley-VCH, **2006**.
- [22] U. Resch-Genger, M. Grabolle, S. Cavaliere-Jaricot, R. Nitschke, T. Nann, *Nat. Methods* **2008**, *5*, 763–775.
- [23] J. R. Lakowicz, *Principles of Fluorescence Spectroscopy*, 3rd ed., Springer, Singapore, **2006**.
- [24] A. M. Smith, H. Duan, A. M. Mohs, S. Nie, *Adv. Drug Delivery Rev.* **2008**, *60*, 1226–1240.
- [25] a) R. Gill, I. Willner, I. Shweky, U. Banin, *J. Phys. Chem. B* **2005**, *109*, 23715–23719; b) C.-Y. Zhang, H.-C. Yeh, M. T. Kuroki, T.-H. Wang, *Nat. Mater.* **2005**, *4*, 826–831; c) H. Zhang, P. G. Stockley, D. Zhou, *Faraday Discuss.* **2011**, *149*, 319–332; d) X. Wang, X. Lou, Y. Wang, Q. Guo, Z. Fang, X. Zhong, H. Mao, Q. Jin, L. Wu, H. Zhao, J. Zhao, *Biosens. Bioelectron.* **2010**, *25*, 1934–1940; e) G. Jiang, A. S. Susha, A. A. Lutich, F. D. Stefani, J. Feldmann, A. L. Rogach, *ACS Nano* **2009**, *3*, 4127–4131.
- [26] a) J. Lee, Y. Choi, J. Kim, E. Park, R. Song, *ChemPhysChem* **2009**, *10*, 806–811; b) X. Li, J. Qian, L. Jiang, S. He, *Appl. Phys. Lett.* **2009**, *94*; c) L. Dyadyusha, H. Yin, S. Jaiswal, T. Brown, J. J. Baumberg, F. P. Booy, T. Melvin, *Chem. Commun.* **2005**, 3201–3203.
- [27] G. Giraud, H. Schulze, T. T. Bachmann, C. J. Campbell, A. R. Mount, P. Ghazal, M. R. Khondoker, S. W. J. Ember, I. Ciani, C. Tlili, A. J. Walton, J. G. Terry, J. Crain, *Chem. Phys. Lett.* **2010**, *484*, 309–314.
- [28] J. K. Jaiswal, E. R. Goldman, H. Mattoussi, S. M. Simon, *Nat. Methods* **2004**, *1*, 73–78.
- [29] J. B. Delehanty, H. Mattoussi, I. L. Medintz, *Anal. Bioanal. Chem.* **2009**, *393*, 1091–1105.
- [30] F. Chen, D. Gerion, *Nano Lett.* **2004**, *4*, 1827–1832.
- [31] K. Boeneman, J. B. Delehanty, K. Susumu, M. H. Stewart, I. L. Medintz, *J. Am. Chem. Soc.* **2010**, *132*, 5975–5977.
- [32] X. Gao, Y. Cui, R. M. Levenson, L. W. K. Chung, S. Nie, *Nat. Biotechnol.* **2004**, *22*, 969–976.
- [33] a) H. M. E. Azzazy, M. M. H. Mansour, S. C. Kazmierczak, *Clin. Biochem.* **2007**, *40*, 917–927; b) A. M. Smith, X. Gao, S. Nie, *Photochem. Photobiol.* **2004**, *80*, 377–385.
- [34] P. Chan, T. Yuen, F. Ruf, J. Gonzalez-Maeso, S. C. Sealson, *Nucl. Acids Res.* **2005**, *33*, e161.
- [35] C. Chatgililoglu, D. Griller, M. Lesage, *J. Org. Chem.* **1989**, *54*, 2492–2494.
- [36] R. S. Tanke, S. M. Kauzlarich, T. E. Patten, K. A. Pettigrew, D. L. Murphy, M. E. Thompson, H. W. H. Lee, *Chem. Mater.* **2003**, *15*, 1682–1689.
- [37] A. Shiohara, S. Hanada, S. Prabakar, K. Fujioka, T. H. Lim, K. Yamamoto, P. T. Northcote, R. D. Tilley, *J. Am. Chem. Soc.* **2009**, *132*, 248–253.
- [38] a) M. Rosso-Vasic, L. De Cola, H. Zuilhof, *J. Phys. Chem. C* **2009**, *113*, 2235–2240; b) M. Rosso-Vasic, E. Spruijt, Z. Popovic, K. Overgaag, B. van Lagen, B. Grandidier, D. Vanmaekelbergh, D. Dominguez-Gutierrez, L. De Cola, H. Zuilhof, *J. Mater. Chem.* **2009**, *19*, 5926–5933.
- [39] L. Wang, V. Reipa, J. Blasic, *Bioconjugate Chem.* **2004**, *15*, 409–412.
- [40] a) H. C. Kolb, M. G. Finn, K. B. Sharpless, *Angew. Chem.* **2001**, *113*, 2056–2075; *Angew. Chem. Int. Ed.* **2001**, *40*, 2004–2021; b) R. K. Iha, K. L. Wooley, A. M. Nyström, D. J. Burke, M. J. Kade, C. J. Hawker, *Chem. Rev.* **2009**, *109*, 5620–5686; c) C. Remzi Becer, R. Hoogenboom, U. S. Schubert, *Angew. Chem.* **2009**, *121*, 4998–5006; *Angew. Chem. Int. Ed.* **2009**, *48*, 4900–4908.
- [41] a) T. Posner, *Ber. Dtsch. Chem. Ges.* **1905**, *38*, 646–657; b) C. E. Hoyle, T. Y. Lee, T. Roper, *J. Polym. Sci. Part A* **2004**, *42*, 5301–5338.
- [42] a) A. Dondoni, *Angew. Chem.* **2008**, *120*, 9133–9135; *Angew. Chem. Int. Ed.* **2008**, *47*, 8995–8997; b) C. E. Hoyle, C. N. Bowman, *Angew. Chem.* **2010**, *122*, 1584–1617; *Angew. Chem. Int. Ed.* **2010**, *49*, 1540–1573.
- [43] C. E. Hoyle, A. B. Lowe, C. N. Bowman, *Chem. Soc. Rev.* **2010**, *39*, 1355–1387.
- [44] a) A. W. Harant, V. S. Khire, M. S. Thibodaux, C. N. Bowman, *Macromolecules* **2006**, *39*, 1461–1466; b) M. A. Caipa Campos, J. M. J. Paulusse, H. Zuilhof, *Chem. Commun.* **2010**, *46*, 5512–5514; c) P. Jonkheijm, D. Weinrich, M. Kohn, H. Engelkamp, P. C. M. Christmanen, J. Kuhlmann, J. C. Maan, D. Nüsse, H. Schroeder, R. Wacker, R. Breinbauer, C. M. Niemeyer, H. Waldmann, *Angew. Chem.* **2008**, *120*, 4493–4496; *Angew. Chem. Int. Ed.* **2008**, *47*, 4421–4424.

- [45] a) N. ten Brummelhuis, C. Diehl, H. Schlaad, *Macromolecules* **2008**, *41*, 9946–9947; b) L. M. Campos, K. L. Killops, R. Sakai, J. M. J. Paulusse, D. Damiron, E. Drockenmuller, B. W. Messmore, C. J. Hawker, *Macromolecules* **2008**, *41*, 7063–7070.
- [46] a) K. L. Killops, L. M. Campos, C. J. Hawker, *J. Am. Chem. Soc.* **2008**, *130*, 5062–5064; b) T. Kang, R. J. Amir, A. Khan, K. Ohshimizu, J. N. Hunt, K. Sivanandan, M. I. Montanez, M. Malkoch, M. Ueda, C. J. Hawker, *Chem. Commun.* **2010**, *46*, 1556–1558.
- [47] a) M. J. Kade, D. J. Burke, C. J. Hawker, *J. Polym. Sci. Part A* **2010**, *48*, 743–750; b) L. M. Campos, I. Meinel, R. G. Guino, M. Schierhorn, N. Gupta, G. D. Stucky, C. J. Hawker, *Adv. Mater.* **2008**, *20*, 3728–3733.
- [48] L. Ruizendaal, U. Chinnaswamy, L. Voorhaar, J. M. J. Paulusse, H. Zuilhof, **2011**, manuscript in preparation.
- [49] J. A. Kelly, E. J. Henderson, R. J. Clark, C. M. Hessel, R. G. Cavell, J. G. C. Veinot, *J. Phys. Chem. C* **2010**, *114*, 22519–22525.
- [50] W. W. Yu, L. Qu, W. Guo, X. Peng, *Chem. Mater.* **2003**, *15*, 2854–2860.
- [51] W. D. A. M. de Boer, D. Timmerman, K. Dohnalova, I. N. Yassievich, H. Zhang, W. J. Buma, T. Gregorkiewicz, *Nat. Nanotechnol.* **2010**, *5*, 878–884.
- [52] A. T. R. Williams, S. A. Winfield, J. N. Miller, *Analyst* **1983**, *108*, 1067–1071.
- [53] D. Jurbergs, E. Rogojina, L. Mangolini, U. Kortshagen, *Appl. Phys. Lett.* **2006**, *88*, 233116–233118.
- [54] R. Anthony, U. Kortshagen, *Phys. Rev. B* **2009**, *80*, 115407–115412.
- [55] F. A. Reboredo, G. Galli, *J. Phys. Chem. B* **2005**, *109*, 1072–1078.

Received: April 13, 2011
Published online: August 24, 2011